Top. Meteor. Oceanogr., 5(1): 67-78, 1998

Impact of horizontal resolution in the generation and evolution of potential vorticity and vertical vorticity in orographic flows

Jorge A. Gutiérrez C.[1]

Laboratorio de Investigaciones Atmosféricas y Planetarias y
Centro de Investigaciones Geofísicas, Universidad de Costa Rica

(Recibido 29 de marzo 1998, aceptado 22 de mayo 1998)

Abstract

The impact of horizontal resolution in a limited area numerical model is investigated. It is found that an increase of horizontal resolution yields larger values for the potential vorticity field and the vertical vorticity field. The structure of the zonal and meridional components of the vorticity field is altered and these fields present larger extrema.

1. Introduction

Orographic flows present a great challenge to researchers due to their complexity, wide range of dynamical behaviour and their impact on air transport, pollutant dispersion, enhancement of rain and structural damage to nearby buildings located on the lee of the obstacle.

The non-linearity of the physical processes involved in orographic flow dynamics does not allow the simplification of the equations of motion. This leads researchers in the field to

[1] Corresponding author address: Dr. Jorge A. Gutiérrez C., Escuela de Física, Universidad de Costa Rica, San Pedro, 2060, Costa Rica.
Email: jgutier@ariel.efis.ucr.ac.cr

perform experiments under controlled conditions by means of numerical models, laboratory experiments in wind tunnels or towing tanks and field experiments.

An understanding of orographic flows is also needed in order to improve the quality of weather forecasts. These numerical weather prediction models need to properly represent mountain effects with the object to parametrise them in an appropiate way in order to yield a reliable forecast.

The accurate forecast of precipitation over complex topography is also a very difficult problem in mountain meteorology. This is an important task for numerical weather prediction but it is a crucial one in hydrologic anf agricultural applications. A short review of experimental, analytical and numerical modeling approaches for meso-gamma scale precipitation can be found in Alpert et al. (1994).

Research on orographic flows is complicated by the existence of a large number of scales that ought to be considered. The disturbance introduced in the flow by a narrow hill will be quite different from that caused by a broad plateau, even if other factors like the terrain height remain the same. This is due to the existence of several natural scales in the atmospheric system with which the mountain width can be compared, some of these are:

1- the distance travelled downwind by an air parcel during a buoyancy oscillation.

2- the distance travelled downstream by an air parcel during the condensation of water droplets and the fallout of precipitation.

3- the depth of the boundary layer.

Field experiments constitute another way of gathering data that will yield some information about orographic flows. An example of these is the Alpine experiment (ALPEX) which has revealed that low-level air is diverted around the Alps without reaching the top of the orography and that the airflow above the summit-level crosses the mountain with little evidence of orographic perturbation (Pierrehumbert and Wyman, 1985). This type of events in which air is diverted around the orography rather than flowing over the obstacle occur when a parameter known as the Froude number is small. The Froude number is defined, in stratified flows as $Fr = U/Nh$ where U is the speed of the wind, N is the Brunt-Väisälä frequency and h is the height of the obstacle.

2. Numerical simulations of orographic flows

In a previous paper Gutiérrez and Thorpe (1997) have shown that the internal diffusion of a numerical model is responsible for the production of potential vorticity even in situations where the initial conditions and boundary conditions of the numerical experiment are such that, physically speaking, no such production of Ertel´s potential vorticity is expected. The potential vorticity, from here onwards will be referred to as PV and is defined as

$$PV = \rho^{-1}\vec{\omega} \bullet \vec{\nabla}\theta \qquad (1)$$

where $\vec{\omega}$ is the vorticity vector, $\omega = \vec{\nabla} \times \vec{V}$, $\vec{\omega} = (\xi, \eta, , \zeta)$. ξ is the zonal component of vorticity, η is the meridional component of vorticity and ζ is the vertical component of vorticity. θ here represents potential temperature.

The results on the production and evolution of PV presented by Gutiérrez and Thorpe (1997) contradict those of Smolarkiewicz and Rotunno (1989) who claimed that no PV was produced in their inviscid simulations. Gutiérrez and Thorpe (1997) attributed the production of potential vorticity in their calculations to internal dissipation of their limited area model. This internal diffusion is caused by the use of horizontal filters employed to eliminate the growth of subgrid scale waves. Rotunno has agreed (personal communication) that PV is produced by the internal dissipation in limited area models.

In this paper the effect on the production of PV and ζ due to an increase of horizontal resolution will be investigated. The model used is a three-dimensional, non-linear, non-hydrostatic model developed by Pedro Miranda at the University of Reading. A description of this model can be found in Gutiérrez (1997).

3. Effects of higher resolution in the generation and evolution of PV and ζ

Crook et al. (1990) found in their investigations of the Denver Cyclone that the computation of the magnitude of vertical vorticity is highly sensitive to the resolution of the simulation. The term Denver Cyclone is employed to describe a mesoscale vortex that forms in the Denver region under certain large scale flow conditions. The frequent formation of this vortex was first noticed in 1981. Since then, several studies have shown that severe weather, in particular tornadic storms, often develop after the formation of a Denver cyclone. Crook and his collaborators observed that when the horizontal resolution of their numerical model was increased by a factor of four then the vertical vorticity increased much faster than in the low resolution simulation and reached a maximum that was approximately four times greater than the results obtained in the low resolution run. They used two ways to approach a low Froude number regime. In both experiments they employed a bell-shaped mountain and a constant background stratification equal to $N = 1 \times 10^{-4} s^{-1}$ and free-slip conditions at the lower boundary.

The numerical model used by Crook et al. (1990) was developed by T. Clark and his collaborators. The model integrates the finite-difference approximations to the anelastic, nonhydrostatic equations governing atmospheric motion. These are set on a non-orthogonal, terrain-following coordinate system. The finite-difference expression of the momentum equations uses the Arakawa-Lilly second-order algorithm and the second-order accurate, positive-definite advection transport of Smolarkiewicz is used for all scalar conservation equations. The resulting algorithm for the evaluation of the entire system of model equations is second-order in time and space.

Boundary conditions used at the upper and lower surfaces are zero-flux for the scalar quantities and, in most of their experiments, free-slip for the velocity components. To reduce gravity wave reflections from the upper boundary, Rayleigh damping is used in the upper one-third of the domain. At the lateral boundaries of the outer model, an open boundary extrapolation scheme is used.

Basically, Crook et al., started in the first experiment, which they named FRDEC, with a flow whose Froude number was equal to 0.8 and reduced the background speed of the flow until until a regime with a Foude number equal to 0.3 was attained. In the second numerical experiment which was called FRINC they started the flow from rest and increased the speed of the flow until a Froude number regime of 0.3 was reached. In FRDEC they found return flow aloft and observed that the region of flow reversal descended all the way to the surface and associated this descent with a highly non-linear wave-breaking process. In FRINC they discovered that return flow was first observed at the ground and that the vortices would gradually deepen with time. Crook et al, concluded that soon after the flow reverses in this experiment the isentropic surfaces nerar the ground overturn and become more horizontal, reducing the upward propagation of energy, eliminating the possibility of wave breaking aloft.

In order to show that wave breaking took place in their simulaion FRDEC Crook et al. performed calculations with higher horizontal resolution. Their reasoning was as follows. The baroclinic mechanism proposed by Smolarkiewicz and Rotunno (1989) depends on gravity waves that have horizontal scales similar to the width of the obstacle, according to Crook et al. The strength of the vorticity field should not change much as there are several gridpoints across the obstacle. This is a debatable point though, since a better-resolved

obstacle is most likely to have an impact on the gravity waves that it may generate, also, they did not specify what they meant by 'several grid points'. Crook et al. claimed that if wavebreaking is important in FRDEC then the strength of the simulated vorticity will depend on the resolution since wavebreaking can produce energy to the smallest scales. To this effect Crook and his collaborators increased the horizontal resolution of their numerical model by a factor of four and obtained a vorticity field that is four times more intense than the vorticity field obtained in the low-resolution experiment. The pattern of vertical vorticity at the reference level (in their experiments this corresponds to the surface) was found to be radically different to the pattern found in their low resolution experiment. The vorticity field obtained in the high resolution experiment is found to be very noisy.

In the high-resolution simulation presented here and performed by means of the Reading Model a horizontal resolution of two kilometres in the zonal and meridional directions was used and a temporal resolution of two seconds was chosen in order to comply with the CFL condition. The experiments without background rotation performed with the Reading Model show that the intensity of the vorticity filed increases by a factor of 4.5 after an increase in the horizontal and temporal resolutions of 7.5. Thus, the increase in the intensity of the vorticity field is not one-to-one with respect to the increase in the spatio-temporal resolution as in experiment FRDEC of Crook et al.. The pattern of the vertical vorticity field obtained in the high-resolution experiment performed with the Reading Model is smooth, which is not the case of the result obtained by Crook et al.

It is also found that the vorticity extrema are located away from the lee of the orography in calculations performed at a height of 400 metres above level ground. The cores of the vortices are located at about forty five kilometres from the mountain's cross section. The vertical vorticity field obtained in the high-resolution experiment is shown in Figure 1.

The same vertical vorticity field plotted using a contour interval of $0.2 \times 10^{-4} s^{-1}$ is shown in Figure 2, this facilitates the comparison with Figure 3, which shows the vertical vorticity field obtained in the low resolution experiment, in which a horizontal grid resolution of 15 kilometres in both the zonal and meridional directions was used. Notice that the vertical vorticity field is smooth in both figures and not noisy as reported in the results of Crook et al (1990). Both Figure 3 and Figure 2 show symmetric areas of cyclonic and anticyclonic vorticity. These areas have similar zonal and meridional dimensions.

One reason why the extrema of vorticity appear to be located away from the orography is due to the way vertical vorticity has bee computed. The computation of the vertical vorticity employed centred differences, thus,

$$\zeta(i,j) = \frac{v(i+1,j) - v(i-1,j)}{2\Delta x} - \frac{u(i,j+1) - u(i,j-1)}{2\Delta y} \qquad (2)$$

When one of the values needed to calculate $\zeta(i,j)$ is not defined because it is inside the area occupied by the cross-section of the mountain the vertical vorticity is not computed at that point. Thus the cross section of the mountain is increased. In the case of the low-resolution experiment the distance between consecutive gridpoints is 15 kilometres whereas in the high resolution experiment it is 2 kilometres and so this increment is of at least 15 kilometres in the low resolution experiment and 2 kilometres in the high resolution experiment.

When the data obtained from the high resolution run is used to perform a 'coarser' calculation of ζ, i.e., computing ζ at every eight gridpoints in order to get a horizontal separation equivalent to that of the low resolution experiment it is found that the values of the vorticity field are halved and that the extrema of the vorticity are located close to the orography.

The structure of the perturbation potential temperature field at 400 metres above level ground

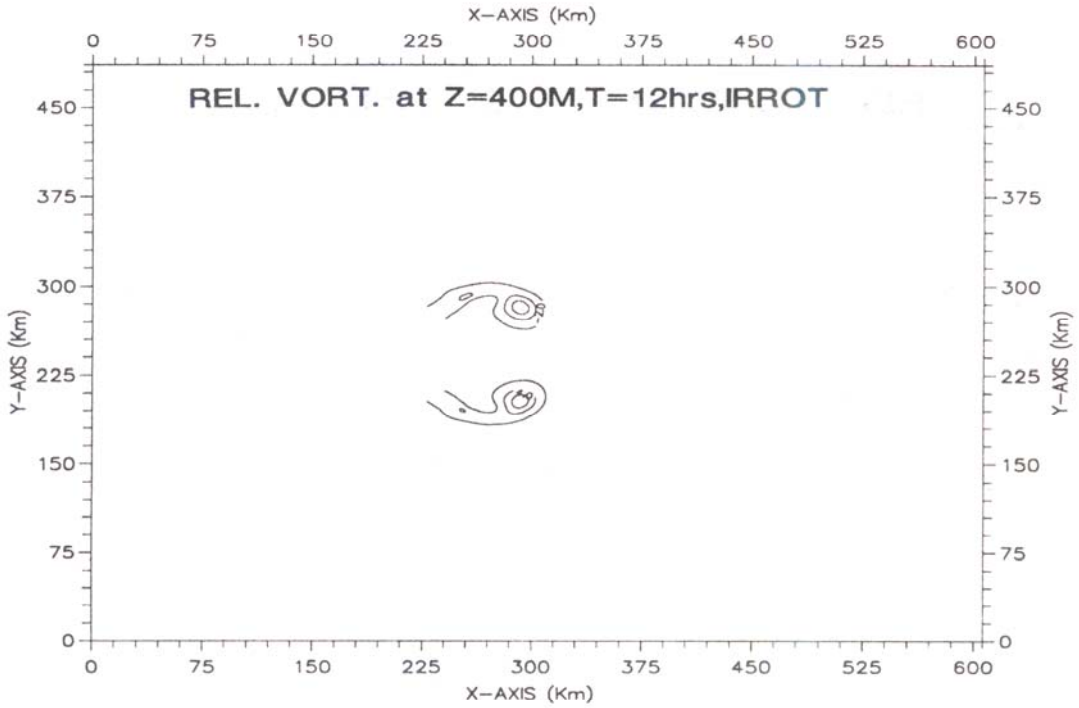

Fig. 1: Vertical vorticity obtained after an integration of twelve hours using a horizontal resolution of dx=dy=2 km and a time-step of two seconds. The vorticity field is shown at 400 metres above level ground. The contour interval is $2.0 \times 10^{-4} s^{-1}$. Inviscid flow without background rotation.

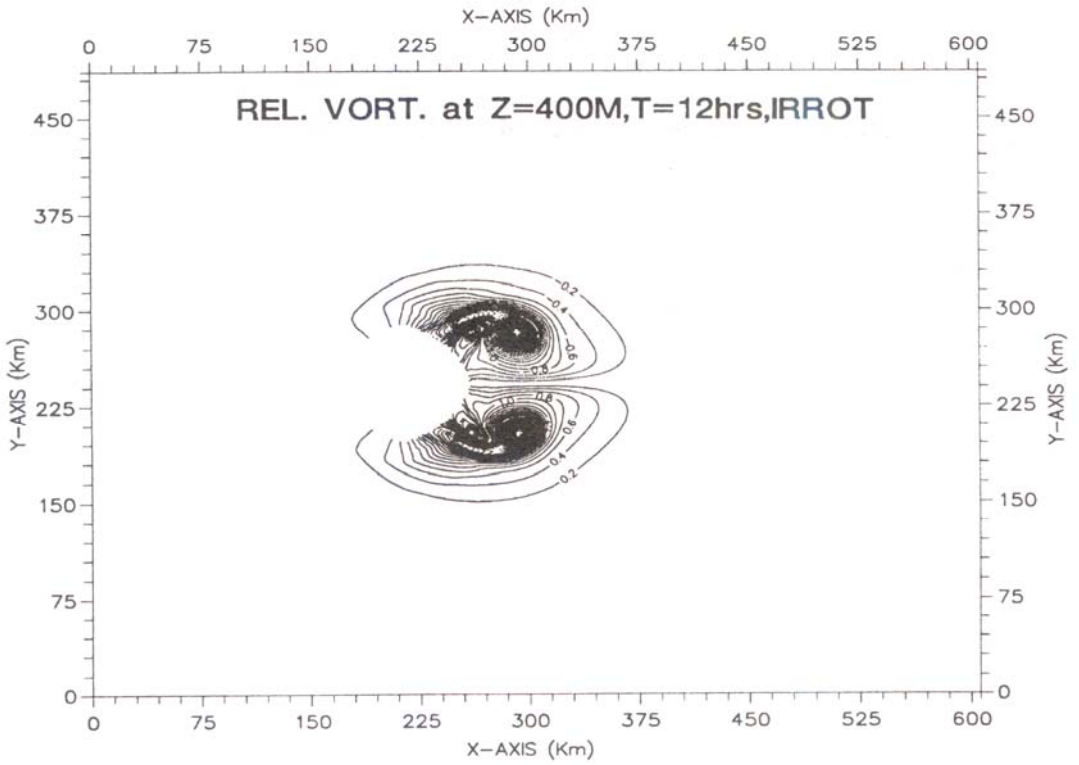

Fig. 2: Vertical vorticity field obtained after a twelve-hour integration using a horizontal resolution of dx=dy= 2 km and a time-step of two seconds. The vorticity field is shown at 400 metres above level ground. The contour interval is $0.2 \times 10^{-4} s^{-1}$. Inviscid flow with background rotation.

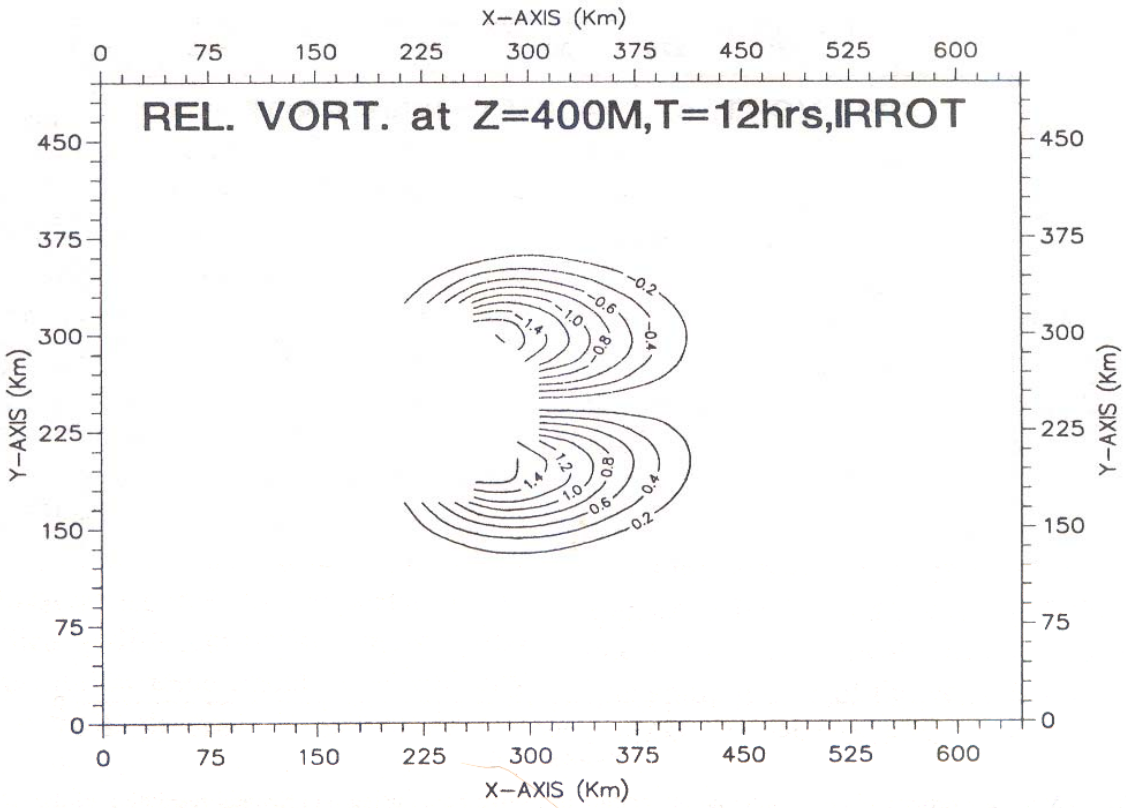

Fig. 3: Relative vorticity field at z=400 metres above level ground. Inviscid flow without background rotation. Integration time 12 hours. Contour interval 02 x 10^{-4} s^{-1}. Fr = 0.2

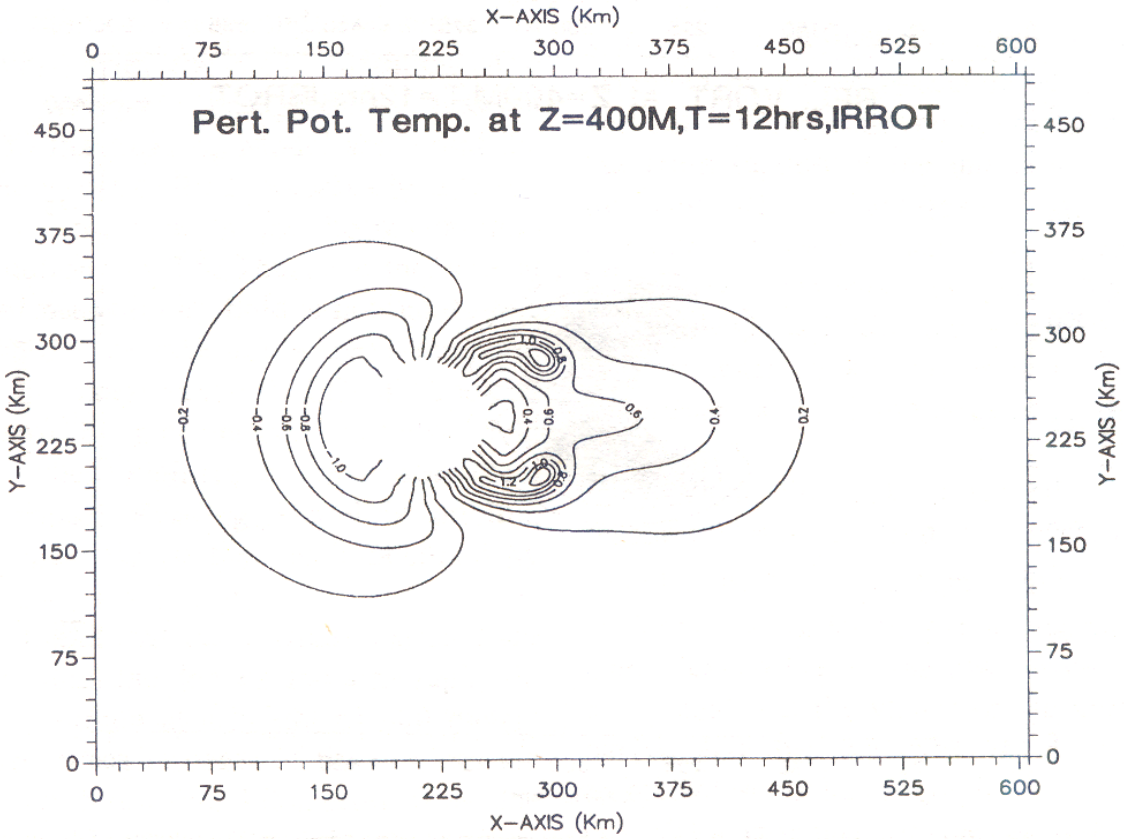

Fig. 4: Potential temperature perturbation at z=400 metres above level ground. High resolution experiment. Contour interval 0.2 K. Integration time twelve hours.

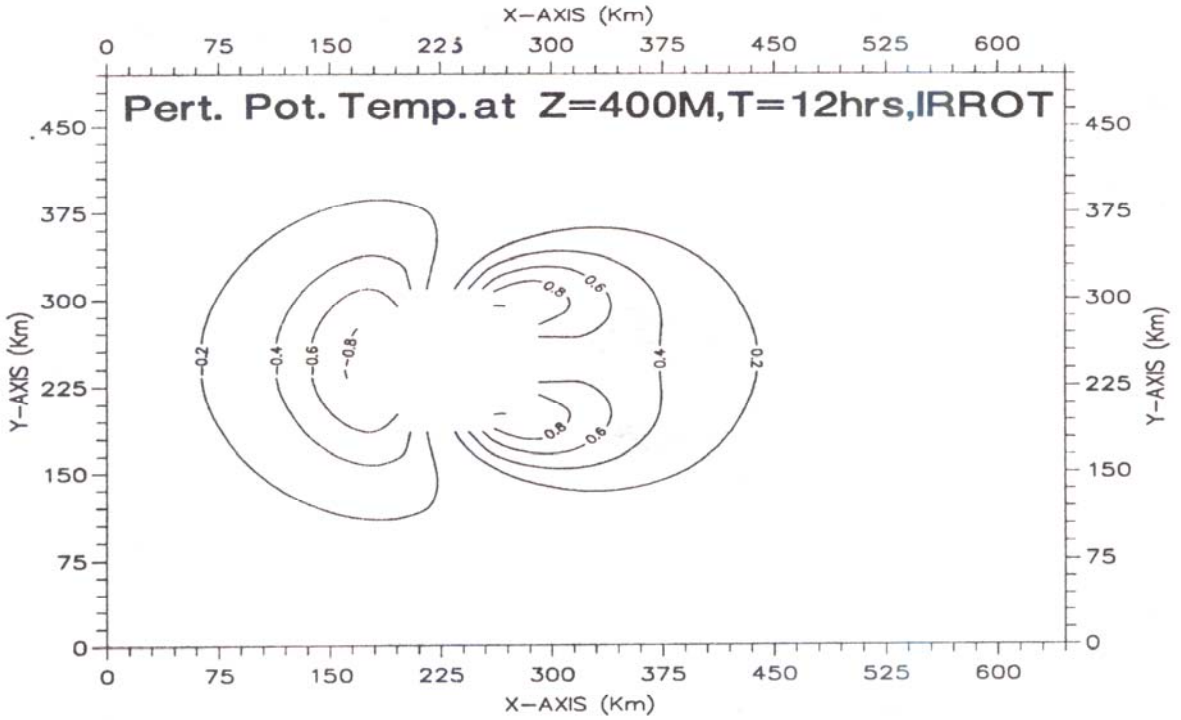

Fig. 5. Potential temperature perturbation at z=400 metres above level ground. Low resolution experiment. Inviscid flow without background rotation. Integration time twelve hours. Contour interval 0.2 K.

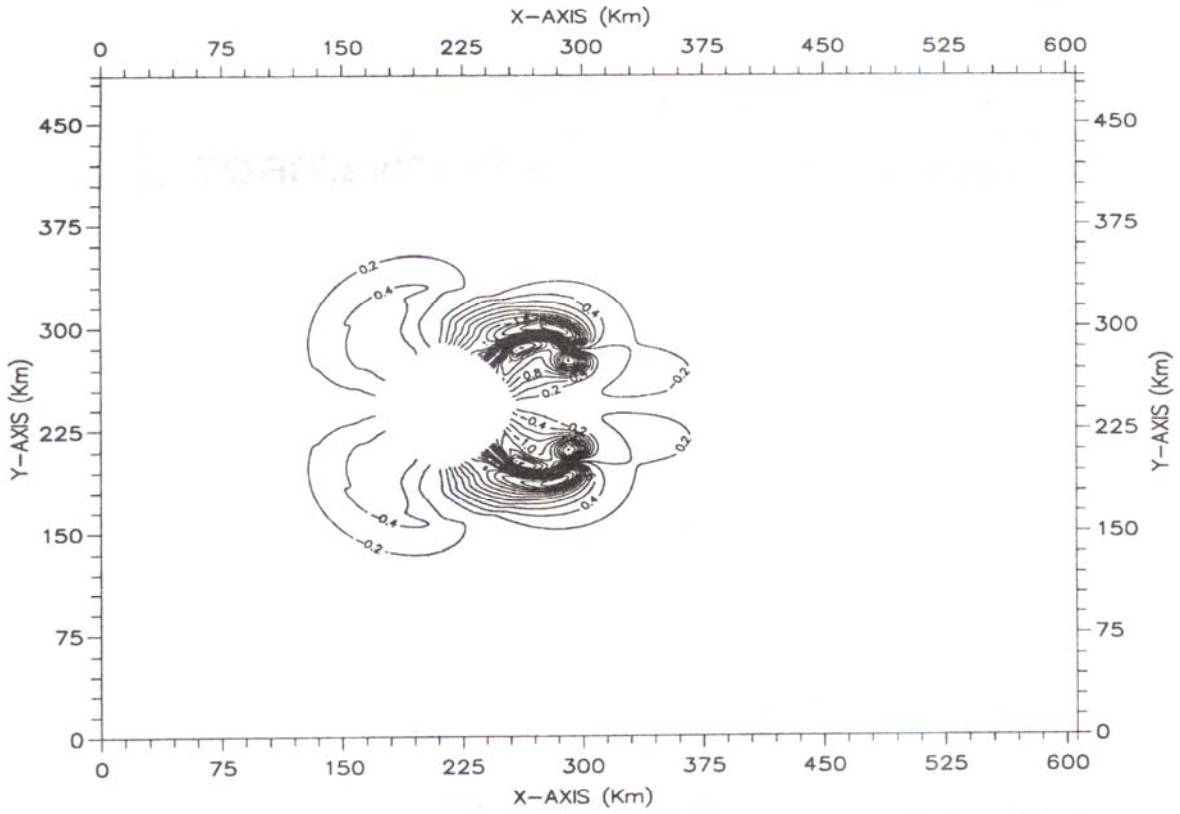

Fig. 6. Rate of production of the zonal component of horizontal vorticity due to the baroclinic term at z=400 metres above level ground. High resolution experiment. Contour interval $0.2 \times 10^{-6} s^{-2}$. Integration time twelve hours.

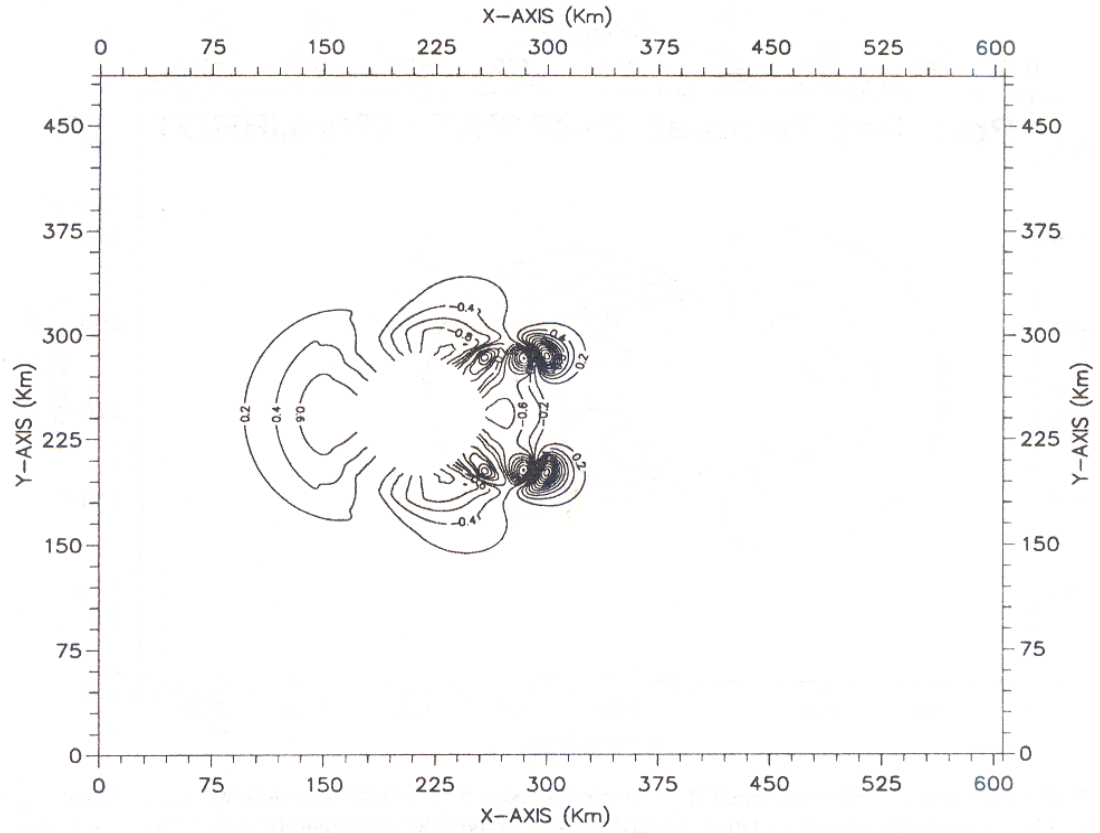

Fig. 7. Rate of production of the meridional component of horizontal vorticity due to the baroclinic mechanism at z=400 metres above level ground. High resolution experiment. Contour interval $0.2 \times 10^{-6} s^{-2}$. Integration time twelve hours.

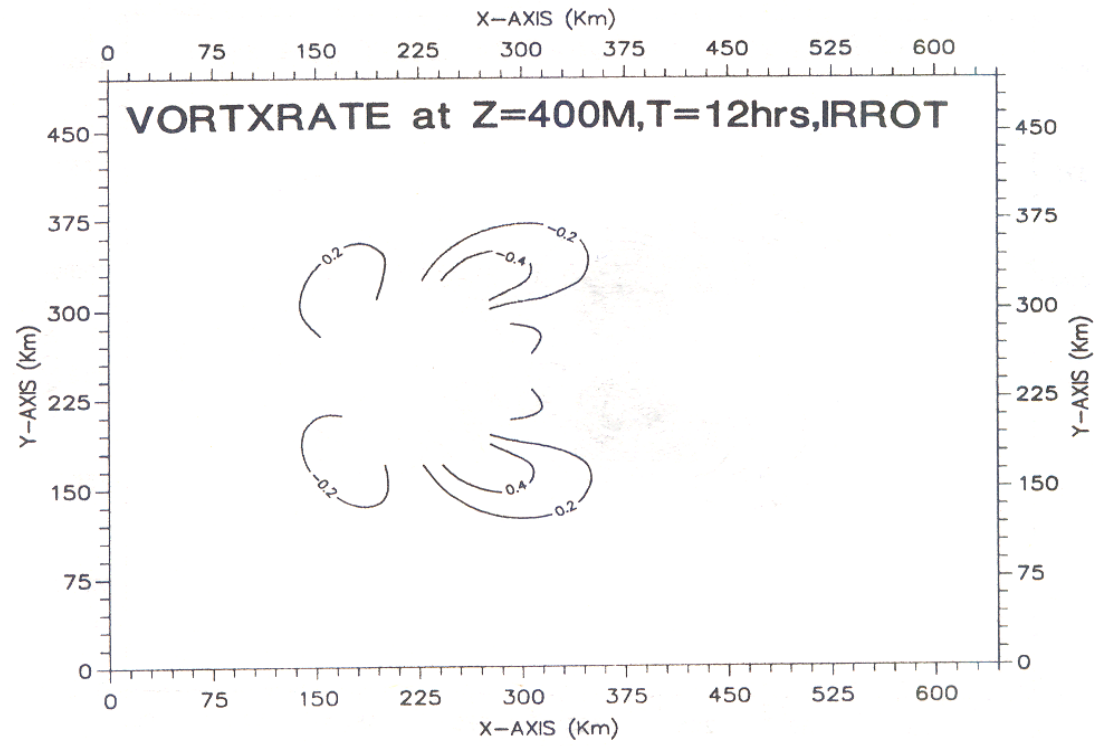

Fig. 8. Rate of production of the zonal component of horizontal vorticity at 400 metres above level ground. Inviscid flow without background rotation. Low resolution experiment. Integration time twelve hours. Contour interval $0.2 \times 10^{-6} s^{-2}$.

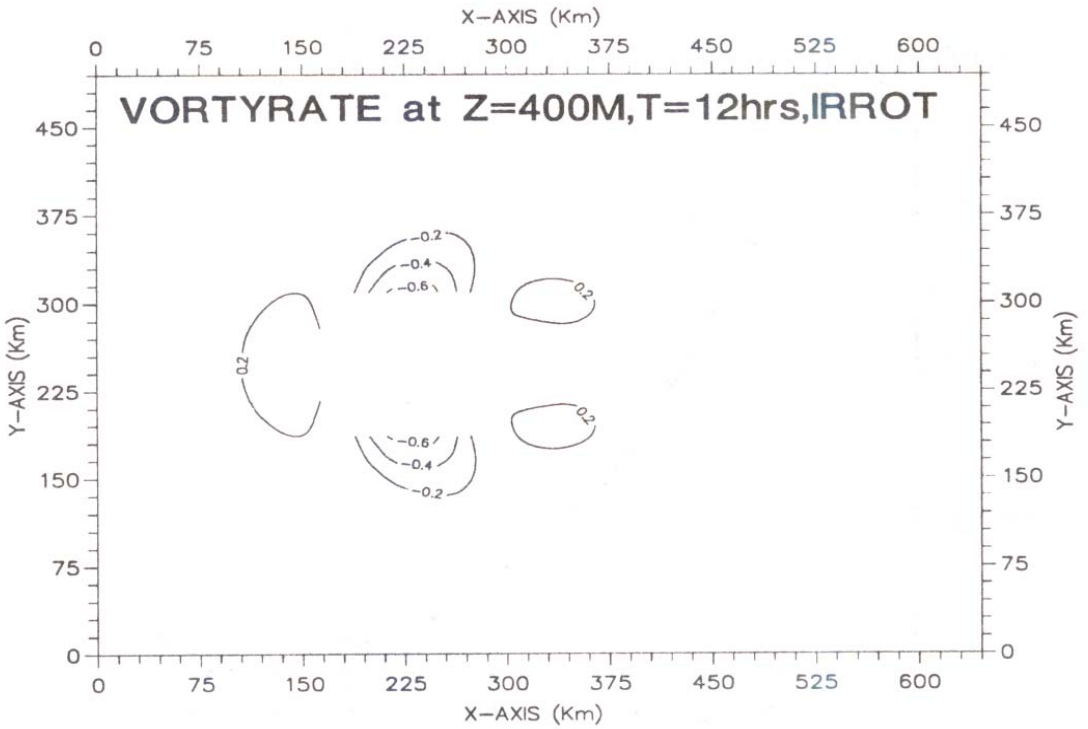

Fig. 9. Rate of production of the meridional component of horizontal vorticity at z=400 metres above level ground. Integration time twelve hours. Contour interval $0.2 \times 10^{-6} s^{-2}$. Low resolution experiment.

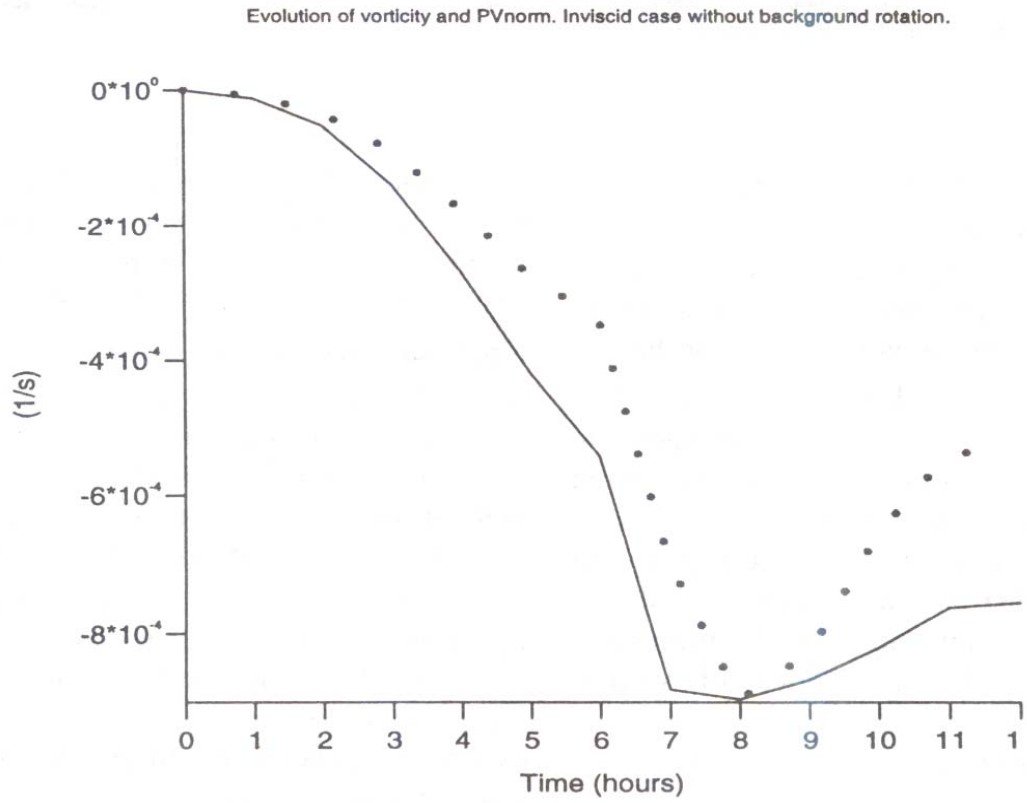

Fig. 10. Evolution of ζ and PVnorm as obtained in the high-resolution experiment. The evolution of the vertical vorticity is shown by the continuous line and that of the normalised potential vorticity corresponds to the dotted line. There are twelve data points taken at a height of 400 metres above level ground in the region of the northern vortex.

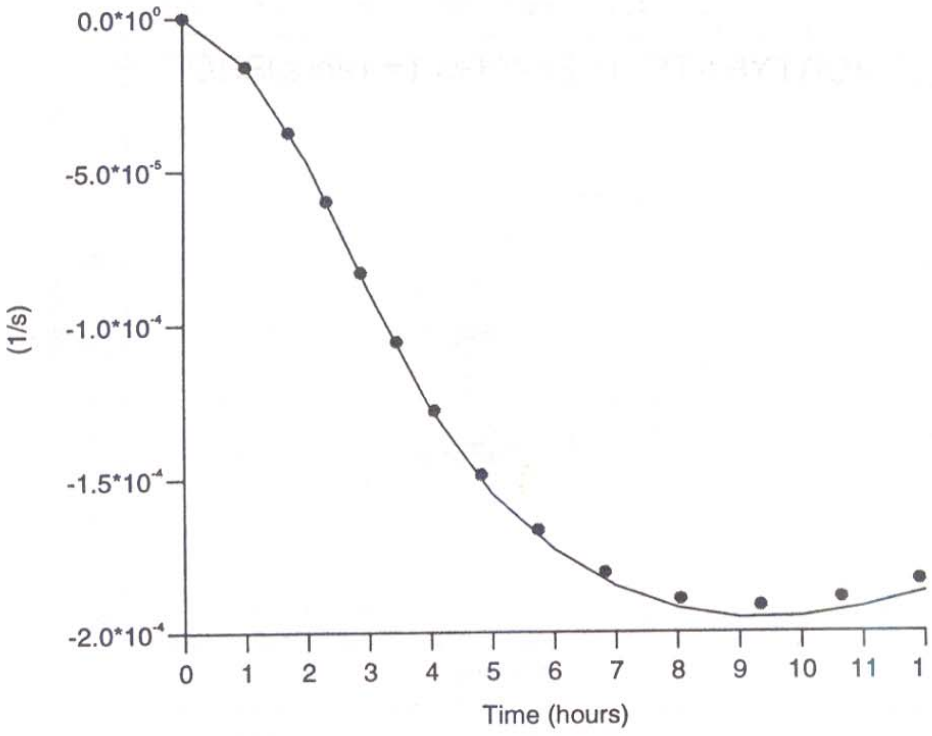

Fig. 11. Evolution of ζ and PVnorm. Inviscid flow without background rotation. Low resolution experiment. The evolution of the vertical vorticity is shown by the continuous line and that of the normalised potential vorticity corresponds to the dotted line. There are twelve data points taken at a height of 400 metres above level ground in the region of the northern vortex.

is shown in Figure 4. It can be seen that the upstream horizontal gradients of θ' here are slightly larger than those obtained in the low resolution experiment which are shown in Figure 5. This explains the larger values of the rate of production of ξ and η shown in Figures 6 and 7 which are more intense than the corresponding values found in the low-resolution experiment which are shown in Figures 8 and 9.

Once horizontal vorticity has been produced the effect of the increase in horizontal resolution will be felt in the computation of the tilting and stretching terms in the production of vertical vorticity.

The rate of production of ξ by the baroclinic mechanism is shown in Figure 6. The basic structure of this field, that is, the location of the areas of positive and negative values of ξ is similar to that shown in Figure 8 which shows the result of the same calculation in the low resolution experiment. The main differences appear in the central area of the wake where the return flow is forced to ascend the lee slope. The values of ξ on the upstream side of the orography are similar to those found in the same location in the low resolution experiment, whereas those on the lee are much stronger in the high resolution calculations.

The rate of production of η by the baroclinic mechanism is shown in Figure 7. The locations of the relative maxima and minima of this field are found at the same locations in both the high resolution experiment and in the low resolution experiment. The main differences appear in the central area of the wake.

Now the evolution of the normalised potential vorticity PVnorm and the vertical

component of the relative vorticity ζ will be investigated.

A normalised potential vorticity was introduced by Gutiérrez and Thorpe (1997), in order to investigated the joint evolution of Ertel's potential vorticity and the vertical component of vorticity. PVnorm was defined by Gutiérrez and Thorpe as

$$PVnorm = \frac{\rho_o PV}{\frac{\partial \bar{\theta}}{\partial z}} \qquad (3)$$

Where ρ_o is a constant at any constant height level. The physical interpretation of Pvnorm is that it is the absolute vorticity the air would have if the static stability were to be equal to a reference constant stability, $\partial \bar{\theta} / \partial z$. This is in accord with Rossby's original definition of potential vorticity. Notice that PVnorm and ζ have the same units which facilitates comparison of these two fields.

The evolution of PVnorm and ζ has been investigated and is shown in Figure 10. There are 12 data points for each field in this figure. The data shown correspond to the extreme values of the fields at a height of 400 metres above level ground. Even though larger values of vorticity and normalised potential vorticity were obtained return flow was observed after four hours of integration which is the same amount of time needed for the formation of return flow in the low resolution simulation.

It is possible that the larger amounts of vertical vorticity obtained in the calculations performed with higher resolution are due to a decrease in the numerical damping of the model via the use of horizontal filters.

An important point related to the result of this higher resolution experiment is that the normalised potential vorticity is observed again to be produced since early in the integration of the model equations, which stresses the point presented in Gutiérrez and Thorpe (1997), that it is not necessary to have fully developed vortices in order to start producing potential vorticity anomalies in the flow.

The evolution of the normalised potential vorticity shown in Figure 10 differs with respect to the one obtained in the experiment with lower resolution, Figure 11, because it is slightly superseded by the production of vertical vorticity. The weak divergence in the evolution of the vertical vorticity and the potential vorticity at the tail of the evolution curve obtained in the low-resolution simulation is wider in the high-resolution case.

4. Conclusions

The production of vertical vorticity and potential vorticity is found to be sensitive to the resolution of the model. Larger values of these fields were found when a higher resolution calculation was performed. This shows, contrary to the supposition of Crook et al. (1990), that a better horizontal resolution has an impact on the baroclinic mechanism.

Even though ζ is found to increase in the experiment with high horizontal resolution the field obtained is smooth rather than noisy as in the results of Crook et al (1990). This is due to the fact that ζ is due to the tilting in the vertical, and the stretching of this vertical vorticity, of baroclinically generated horizontal vorticity whereas in Crook et al.'s experiment ζ is the result of gravity wave breaking.

In spite of higher horizontal resolution PVnorm is still produced since the start of the simulation. This shows that the internal diffusion of the model is still important even though a higher horizontal resolution has been employed.

RESUMEN

Se investiga el impacto de un aumento de la resolución horizontal en la producción de PVnorm y ζ en experimentos de flujos invíscidos con bajo número de Froude. Se encuentra que los campos de PVnorm y ζ son más intensos que aquellos obtenidos en

experimentos de baja resolución. La estructura horizontal de las componentes meridional y zonal del campo de vorticidad difiere de la encontrada en experimentos numéricos con baja resolución.

References

Alpert, P., H. Shafir and H.R. Cotton, 1994. Prediction of meso-γ scale orographic precipitation. *Trends in Hydrology, I (1994),* 403-441.

Crook, N., T. Clark and M.W. Moncrieff, 1990. The Denver Cyclone. Part I: Generation in low Froude-number flow. *Journal of the Atmosperic Sciences, 47, No 23,* 2725-2742.

Gutiérrez, J.A. and A.J. Thorpe, 1997. Low Froude number stratified flows interacting with an isolated obstacle. *Tópicos Meteorológicos y Oceanográficos, 4(2),* 109-128.

Gutiérrez, J.A., 1997. Description of a mesoscale (limited area) numerical model. *Tópicos Meteorológicos y Oceanográficos, 4(2),* 97-107.

Pierrehumbert, R.T. and B. Wyman, 1985. Upstream effects of mesoscale mountains. *Journal of the Atmospherics Sciences, 42, No 10,* 977-1003.

Smolarkiewicz, P. and R. Rotunno, 1989. Low Froude number flow past three-dimensional obstacles. Part I: Baroclinically generated lee-vortices. *Journal of the Atmospheric Sciences, 46, No 23,* 1154-1164.